Spatial and temporal variability of pCO$_2$ and CO$_2$ emissions from the Dongjiang River in South China

Boyi Liu[1], Mingyang Tian[2], Kaimin Shih[3], Chun Ngai Chan[1], Xiankun Yang[4], Lishan Ran[1,*]

[1]Department of Geography, the University of Hong Kong, Hong Kong SAR, China
[2]Institute for Geology, Center for Earth System Research and Sustainability (CEN), Universität Hamburg, Hamburg, Germany
[3]Department of Civil Engineering, the University of Hong Kong, Hong Kong SAR, China
[4]School of Geographical Sciences, Guangzhou University, Guangzhou,510006, China

[*] *Correspondence to*: Lishan Ran (lsran@hku.hk)

Abstract. CO$_2$ efflux at the water–air interface is an essential component of the riverine carbon cycle. However, the lack of spatially resolved CO$_2$ emission measurements prohibits reliable estimation of the global riverine CO$_2$ emissions. By deploying floating chambers, seasonal changes in river water CO$_2$ partial pressure (pCO$_2$) and CO$_2$ emissions from the Dongjiang River in South China were investigated. Spatial and temporal patterns of pCO$_2$ were mainly affected by terrestrial carbon inputs (i.e., organic and inorganic carbon) and in-stream metabolism, both of which varied due to different land cover, catchment topography, and seasonality of precipitation and temperature. Temperature-normalized gas transfer velocity (k_{600}) in small rivers were 8.29 ± 11.29 m d^{-1} and 4.90 ± 3.82 m d^{-1} for the wet season and dry season, respectively, which were nearly 70 % higher than that of large rivers (3.90 ± 5.55 m d^{-1} during the wet season and 2.25 ± 1.61 m d^{-1} during the dry season). A significant correlation was observed between k_{600} and flow velocity but not wind speed regardless of river size. Most of the surveyed rivers were net CO$_2$ source while exhibiting substantial seasonal variations. The mean CO$_2$ flux was 300.1 and 264.2 mmol m^{-2} d^{-1} during the wet season for large and small rivers, respectively, 2-fold larger than that during the dry season. However, no significant difference in CO$_2$ flux was observed between small and large rivers. The absence of commonly observed higher CO$_2$ fluxes in small rivers could be associated with the depletion effect caused by abundant and consistent precipitation in this subtropical monsoon catchment.

1 Introduction

River networks act as a processor that transfers and emits the carbon entering the water, rather than just a passive pipe that transports carbon from the terrestrial ecosystem to the ocean (Cole et al., 2007; Battin et al., 2009; Drake et al., 2018). CO_2 emissions at the water–air interface are an essential component of the riverine carbon cycle. CO_2 emitted from inland waters to the atmosphere reaches up to 2.9 Pg C yr^{-1}, surpassing that transported from land to ocean through rivers (Sawakuchi et al., 2017; Drake et al., 2018). Understanding the role that rivers play in the global carbon cycle is still hindered by uncertainty on the flux estimate of CO_2 emissions from rivers (Cole et al., 2007; Raymond et al., 2013; Sawakuchi et al., 2017; Drake et al., 2018). Riverine carbon emissions have significant temporal and spatial variations, making it challenging to accurately quantify carbon emissions. In addition, watershed geomorphology, hydrological conditions, climate, and other environmental factors can affect the CO_2 efflux in rivers (Alin et al., 2011; Abril et al., 2014; Almeida et al., 2017; Ran et al., 2017a; Borges et al., 2018). Thus, there are substantial differences in CO_2 efflux among rivers in different climate regions, or the same river but between different seasons (Denfeld et al., 2013; Rasera et al., 2013). An enhanced understanding of the temporal and spatial characteristics of the water–air CO_2 flux will facilitate a more robust estimate. However, global riverine CO_2 emission estimates were largely based on data disproportionately focusing on temperate and boreal regions, including North America and Europe (Raymond et al., 2013; Lauerwald et al., 2015; Drake et al., 2018). More studies are required in other data-poor regions to achieve a more accurate estimate.

Rivers in tropical and subtropical regions of East Asia and Southeast Asia are among those underrepresented regions that need more attention since they are essential participants in riverine carbon transport (Ran et al., 2015; Ran et al., 2017b; Drake et al., 2018). The high temperature in this region facilitates a high net primary productivity in the terrestrial ecosystem and intense biochemical activities; both contribute to the carbon input dynamic from soil to rivers (Li et al., 2018). Meanwhile, rivers in this region are under the heavy influence of monsoon climate, and riverine CO_2 emissions vary significantly among seasons due to the changes in temperature and precipitation. In addition, different rivers in this region may have contrasting trends in CO_2 dynamic due to different underlying controlling factors. Some rivers have the highest CO_2 efflux in the wet season (Li et al., 2013; Le et al., 2018; Ni et al., 2019), while others have the highest CO_2 efflux in the dry season (Luo et al., 2019), suggesting that an increase in the wet season runoff can have two distinct consequences. On one hand, recent studies have indicated

that the increased runoff could enhance external carbon inputs and thus CO_2 emissions (Hope et al., 2004; Johnson et al., 2008). On the other hand, the increased runoff may result in a dilution of the dissolved CO_2 in rivers and accordingly a reduction in CO_2 emissions (Ran et al., 2017b; Li et al., 2018). Therefore, it is important to investigate the underlying processes that determine the diverse responses of CO_2 emissions to the monsoon climate.

The Dongjiang River (DJR), located in the subtropical South China, is one of the three tributaries of the Pearl River. Previous studies on riverine carbon transport and emissions in the Pearl River system mainly focused on the Xijiang River, which is characterized by widely distributed carbonate rocks, and the estuary area of the Pearl River Delta (Yao et al., 2007; Zhang et al., 2015; Zhang et al., 2019; Liang et al., 2020). Although some studies on chemical weathering and dissolved inorganic carbon transport in the Dongjiang River basin (DJRB) have been conducted (Tao et al., 2011; Fu et al., 2014), there is still a lack of understanding of the characteristics of catchment-wide CO_2 emissions from the DJRB. Furthermore, a predominantly hilly landscape combined with abundant precipitation favours the formation of a great number of small rivers in the DJRB (Ding et al., 2015). However, current estimates of basin-wide CO_2 emissions from the river network are mostly based on the data from large rivers, and small rivers are heavily underrepresented (Raymond et al., 2013; Drake et al., 2018). Because the controlling factors and the input of carbon could be significantly different between large and small rivers (Johnson et al., 2008; Dinsmore et al., 2013; Hotchkiss et al., 2015; Marx et al., 2017), a more comprehensive quantification of CO_2 emissions from small headwater streams is necessary. Therefore, studies on the characteristics of riverine CO_2 emissions from the DJRB should be conducted among river size spectrums, and the impact of monsoon needs to be considered.

By using directly measured river water CO_2 partial pressure (pCO$_2$) and CO_2 emission data from the DJRB and in conjunction with hydrological and physicochemical data, the objectives of this study were to 1) investigate the spatial and temporal pattern of pCO$_2$ and CO_2 emissions along stream size spectrum and 2) examine the differences in hydrological and physicochemical controls on pCO$_2$ and CO_2 emissions between small headwater streams and large rivers. The results of this study will shed light on the underlying controls of the spatial and temporal distribution of riverine pCO$_2$ and support a refined estimate of regional and global carbon budgets.

2 Material and methods

2.1 Site Description

The DJR in South China is one of the three major tributaries of the Pearl River system (Figure 1). It has a 562 km long mainstem channel and a drainage area of 35,340 km^2 (Chen et al., 2011). Due to its subtropical monsoon climate, precipitation in the DJRB exhibits significant seasonal variability (Figure 2a). The multi-annual average precipitation is about 1800 mm, 80 % of which is concentrated during the wet season from April to September. The Boluo Hydrological Gauge is the lowermost gauge of the Dongjiang River mainstem channel, controlling a drainage area of ~23,000 km^2. The multi-annual average water discharge at Boluo Hydrological Gauge is 23.7 km^3 (Zhang et al., 2008). About 80–90 % of the discharge is transported during the wet season (Figure 2b). The landscape is characterized by plains and hills, accounting for 87.3 % of the river basin area (Ding et al., 2015), and the dominant land use of the catchment is highly diverse evergreen forests of broad-leaved and needle-leaved species (Ran et al., 2012; Chen et al., 2013). The impacts of human activities on land use vary among three regions in the DJRB. Urban expansion and agricultural activities have substantially altered the land use in the Lower and Middle Dongjiang River Basin (LDJRB and MDJRB), respectively, while the Upper Dongjiang River Basin (UDJRB) is less affected by human activities (Figure 1).
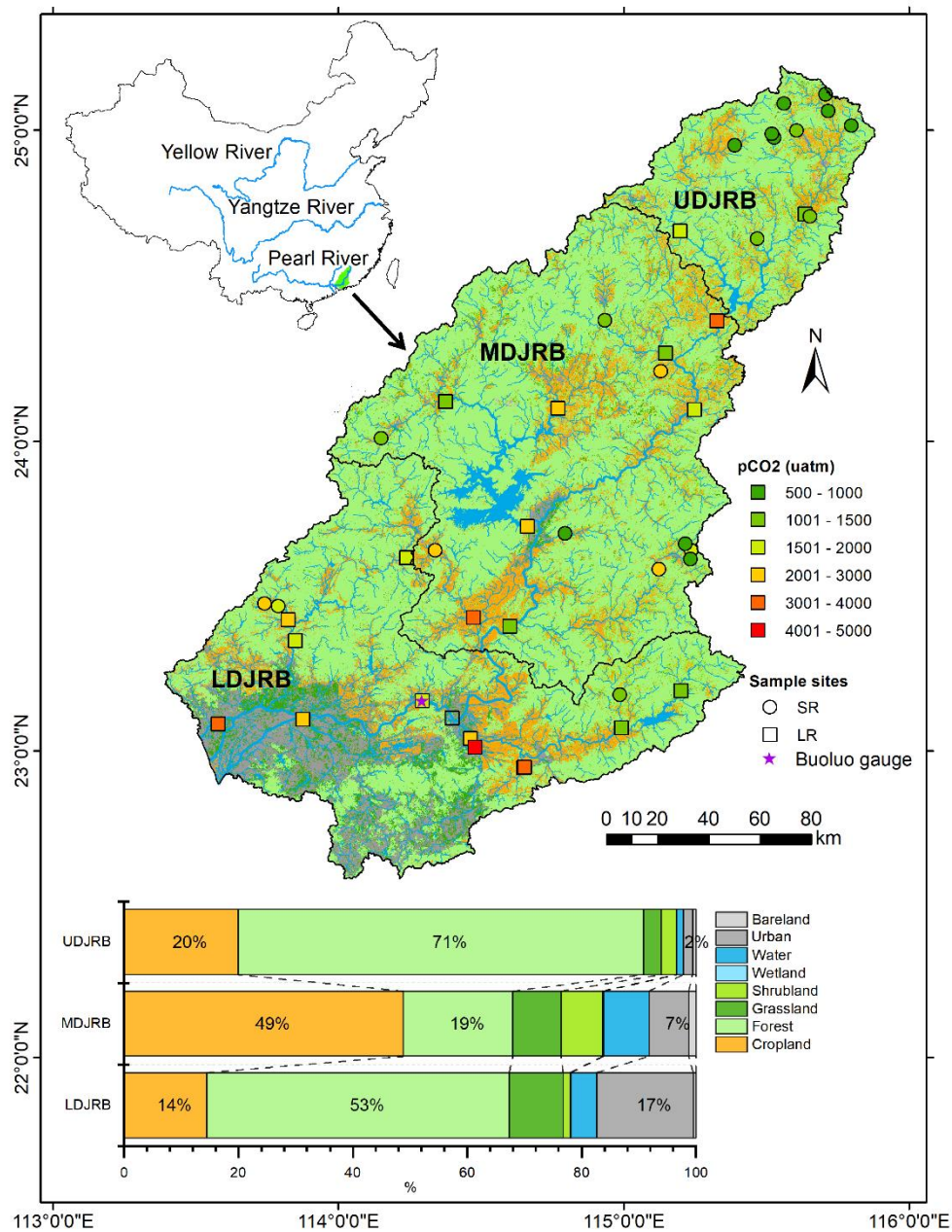
Figure 1 Sample sites and land cover in the DJRB. Yearly average pCO$_2$ at each sample site was displayed. Based on land cover dataset: FROM-GLC10 (http://data.ess.tsinghua.edu.cn).
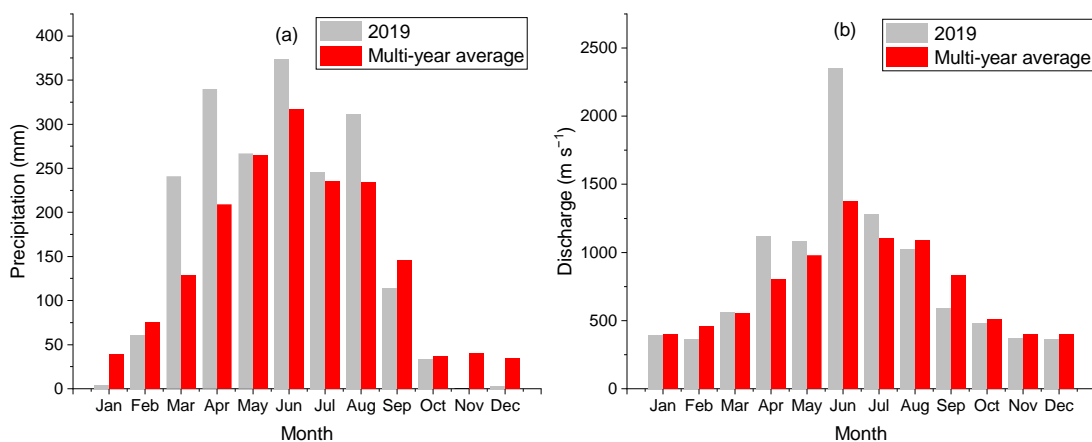
Figure 2 Monthly variations in (a) precipitation of the DJRB and (b) water discharge at the Boluo hydrological gauge, based on data provided by the Hydrological Bureau of Guangdong Province.

2.2 Field Measurements and Analyses

110   In total, there were 43 sampling sites spanning seven Strahler stream orders. Fourth to seven order streams were mainstem and major tributaries, while first to third order streams were small tributaries. River widths were measured by a laser rangefinder. Sampled rivers were categorized, according to their stream orders, into small rivers (first to third order streams, SR) and large rivers (fourth to seventh order streams, LR). The small rivers had an average width of 15.4 ± 10.2 m, while large rivers have an average

115   width of 180.3 ± 159.3 m (Table S1). Those sampling sites were widely distributed in the mainstem and nine major sub-catchments among the three regions with different topographic features and land cover (Figure 1). In order to investigate CO_2 emissions during different hydrological conditions, we performed five fieldwork campaigns from December 2018 to October 2019, including three in the wet season (early wet season - late April, middle wet season - early July, and late wet season - late August) and two in the

120   dry season (middle dry season - December 2018 to early January 2019 and early dry season - late October 2019. Sample sites were measured in the daytime over two weeks for each field trip. Three campaigns in the wet season allowed each sample site to be measured under different hydrological conditions. As for the dry season, the hydrological condition was relatively stable due to low precipitation. However, field measurements conducted during the daytime could lead to an underestimate in pCO$_2$ and CO_2

125   emissions (Reiman and Xu, 2019a). Nocturnal CO_2 emission rates in rivers could be 27% greater than the daytime rates (Gómez-Gener et al., 2021). During the field trips, water temperature, pH, and dissolved

oxygen (DO) were measured with a portable multiparameter probe (Multi 3430, WTW GmbH, Germany). The pH probe was calibrated before each field trip with standard pH buffers (4.01 and 7.00). Measurements were conducted 10 cm below the water surface. To evaluate the contribution of metabolism on DO changes, ΔCO_2 and ΔO_2 were calculated as described by Stets et al. (2017) using:

$$\Delta CO_2 = CO_{2w} - CO_{2a} \tag{1}$$

and

$$\Delta O_2 = O_{2w} - O_{2a} \tag{2}$$

Where, CO_{2w} and O_{2w} are measured concentrations of CO_2 and O_2 in water sample, while CO_{2a} and O_{2a} are the equilibrium CO_2 and O_2 concentrations ($\mu mol\ L^{-1}$).

Flow velocity was determined by using a Global Water Flow Probe FP111 with a precision of 0.1 m s^{-1}, while wind speed at 1.5 m above the water surface was measured with a Kestrel 2500 handheld anemometer and normalized to a height of 10 m (U10) using the equation from Alin et al. (2011). As the flow velocity was measured near the riverbanks, an underestimation of the flow velocity is possible. Flow velocity measured near the riverbanks is only about 40% of the maximum flow velocity at the cross-section (Moramarco et al., 2004; Le Coz et al., 2008). We also collected water for analyzing total alkalinity (TA) and dissolved organic carbon (DOC). Firstly, 100 ml of water samples were filtered through a pre-combusted glass fiber filter (pore size: 0.47 μm, Whatman GF/F, GE Healthcare Life Sciences, USA). Then, 50 ml of water used for TA analysis was titrated with 0.1 mol L^{-1} HCl on the same day of sampling. The remaining 50 ml of water for DOC analysis was poisoned with concentrated H_2SO_4 to pH < 2 and preserved in a cooler with ice bags before analysis. DOC was determined by the high-temperature combustion method using a TOC Analyzer (Elementar Analysensysteme GmbH, Langenselbold, Germany) that has a precision better than 3 %.

2.3 Calculation of pCO$_2$ and CO$_2$ emission flux

The surface water pCO$_2$ was determined using the headspace equilibrium method, which could avoid the possible overestimation of using TA and pH to calculate pCO$_2$ in rivers with a relatively low pH (Abril et al., 2015). We used a 625 mL reagent bottle to collect 400 mL of water from ~10 cm below the surface, leaving 225 mL of space filled with ambient air as headspace. The bottle was then immediately capped and shaken vigorously for at least 1 min to achieve an equilibrium between the water and the CO_2 in the

155 headspace(Hope et al., 1994). Then, the bottle was connected to the calibrated Li-850 CO_2/H_2O gas analyzer (Li-Cor, Inc, USA), and the equilibrated gas in this closed loop was measured. The measurements at each site were repeated twice, and the average was then calculated. The variation between the two measurements was less than 5%, and the accuracy of Li-850 is within 1.5% of the reading. The ambient air pCO_2 (pCO_2^{air}) was measured before the headspace measurements and the

160 chamber deployments. The pCO_2^{air} value varied between 380 and 450 μatm. The original surface water pCO_2 ($pCO_2^{water,i}$) was finally calculated by using solubility constants (K_0) for CO_2 from Weiss (1974), Carbonate constants (K_1, K_2) from (Millero et al., 2006), and the volume of the flask, headspace, and residual system (line and gas analyzer) (Dickson et al., 2007; Ran et al., 2017a; Tian et al., 2019) using:

$$pCO_2^{water,i} = pCO_2^{headspace,f} + (\frac{Vh+Vr}{Vw})(pCO_2^{h+r} - pCO_2^{headspace,i})/[RTK_0(1 + \frac{K_1}{[H+]} + \frac{K_1K_2}{[H+]^2})] \qquad (3)$$

165 Where, V_h, V_r and V_w, are the headspace volume, residence system volume, and water volume, respectively. R is the universal gas constant (8.314 J mol^{-1} K^{-1}), T is the water temperature in Kelvin (K), and [H$^+$] is the concentration of hydrogen ion. $pCO_2^{heasdspace,i}$ and $pCO_2^{headspace,f}$ are pCO_2 before and after the headspace equilibration, respectively. pCO_2^{h+r} is the pCO_2 of the mixed gas in the headspace and residual system during the measurement. the $pCO_2^{headspace,i}$ was taken as the pCO_2 in ambient air

170 before the measurement, while $pCO_2^{headspace,f}$ was calculated using:

$$pCO_2^{headspace,f} = pCO_2^{h+r} + (\frac{V_r}{V_h})(pCO_2^{h+r} - pCO_2^{headspace,i}) \qquad (4)$$

To measure V_r, we filled the headspace with ambient air, which had a known pCO_2, and measured the pCO_2 in the closed loop. V_r was then estimated according to equation (3). A comparative analysis of the syringe and bottle headspace method has been conducted to evaluate the accuracy of the headspace

175 extraction method used in this study (Table S2 and Figure S2). Overall, our method could cause a 1–5% underestimation in pCO_2.

To reduce the artificial turbulence induced by anchored chambers, we used a small unmanned boat in the measurement, which allowed us to deploy drifting chambers freely in rivers deeper than 0.2 m and with a high flow velocity up to 2 m s^{-1}. During the deployment, CO_2 emissions were determined using a

180 circular, 8.5 L floating chamber with a water surface area of 0.113 m^2. The chamber walls were lowered about 2 cm into the water and mounted with a pneumatic rubber tire. The chamber was connected to an

infrared Li-850 CO_2/H_2O gas analyzer (Li-Cor, Inc, USA) in a floating storage box through Polyurethane tubes for CO_2 analysis. An unmanned boat connected to both the chamber and box with ropes was used to deploy them near the central line of the river. Once the entire setup reached its designated location, the readings on the Li-850 were recorded at 0.5 s intervals. During the entire measurement process, the box drifted freely with the current. The Li-850 was calibrated by the manufacturer before field trips. The rate of CO_2 efflux (FCO_2 in mmol m^{-2} d^{-1}) was calculated from the observed change rate of the mole fraction S (ppm s^{-1}) using:

$$FCO_2 = (S \cdot V/A) \cdot t_1 \cdot t_2 \tag{5}$$

Where, S is the slope of CO_2 accumulation in the chamber (µatm s^{-1}), V is chamber gas volume (m^3), A is the chamber area (m^2), t_1 =8.64·10^4 s d^{-1} is the conversion factor from seconds to days, and t_2 is a conversion factor from mole fraction (ppm) to concentration (mmol m^{-3}) at in situ temperature (T in K) and atmospheric pressure (p in Pa), according to the ideal gas law:

$$t_2 = p/(8.31 JK^{-1} mole^{-1} \cdot T) \cdot 1000 \tag{6}$$

The gas transfer velocity (k) was calculated from FCO_2 and pCO_2 in both water and ambient air using:

$$k = FCO_2/(K_0 \cdot (pCO_2^{water,i} - pCO_2^{air})) \tag{7}$$

To compare gas transfer velocity values among different sites, k was standardized to k_{600} as described by Alin et al. (2011) using:

$$k_{600} = k(600/Sc)^{-0.5} \tag{8}$$

Where, Sc is the Schmidt number, which is dependent on temperature (T) in degree Celsius (Wanninkhof, 1992):

$$Sc = 1911.1 - 118.11T + 3.4527T^2 - 0.4132T^3 \tag{9}$$

In total, 196 chamber measurements were conducted. In 19 out of 215 sample sites, the drifting chamber was unable to deploy due to shallow water or high flow velocity. Meanwhile, 8 out of 196 k_{600} data with the air−water pCO_2 gradient less than 200 µatm were also excluded, as the error in these calculations could be considerable (Borges et al., 2004).

3 Results

3.1 Physical and Biochemical Characteristics

The Dongjiang River was characterized by substantial seasonal variations in hydrologic regimes (Figure 2). Stream width in the wet season was 17.0 % and 5.6 % larger than that in the dry season for small and large rivers, respectively (Table S1). The discharge ranged 4 orders of magnitude from 0. 1 m^3 s^{-1} in the small headwater streams during the dry season to 6690 m^3 s^{-1} in the main stem during the wet season (Figure S1). Water temperature was higher in July and August (21.4–33 and 21–33.4 ℃, respectively) than that in January (8.1–22.2 ℃), April (16.5–26.9 ℃), and October (17.4–29.7 ℃). pH varied from 6.38 to 8.14, with a mean of 7.08. There was no significant (independent sample t test, $p > 0.05$) change in pH between wet and dry seasons. U10 based on all stream sites was higher in large rivers (0.86 ± 0.91 and 1.43 ± 1.58 m s^{-1} in wet and dry season, respectively) than in small rivers (0.62 ± 0.61 and 0.76 ± 0.73 m s^{-1} in wet and dry season, respectively).

The streams presented low alkalinity ranging from 225 to 3025 μmol L^{-1}. Overall, lower alkalinity was observed in wet season than in dry season (Table 1). In small rivers, the alkalinity in the wet season (656 ± 265 μmol L^{-1}) was 21.1 % lower than that in the dry season (831 ± 460 μmol L^{-1}), and the lowest alkalinity was observed in April (615 ± 262 μmol L^{-1}), which was 30.4 % lower than in January (883 ± 548 μmol L^{-1}). Similarly, the alkalinity in large rivers was 790 ± 402 μmol L^{-1} in wet season, 14.5 % lower than 924 ± 411 μmol L^{-1} in dry season. However, the lowest value of alkalinity in large rivers was observed in August (739 ± 312 μmol L^{-1}) instead of April in small rivers.

Spatial and seasonal changes in DOC concentration were also observed in the surveyed rivers (Table 1). DOC concentration in large rivers (1.94 ± 1.52 mg L^{-1}) was 41.6 % higher than that in small rivers (1.37 ± 0.72 mg L^{-1}). Meanwhile, DOC concentrations in the wet season were 2.22 ± 1.82 mg L^{-1} and 1.54 ± 0.72 mg L^{-1} for large and small rivers, respectively, which were 45.1 % and 54 % higher than that in the dry season (1.53 ± 0.72 and 1.11 ± 0.63 mg L^{-1} for large and small rivers, respectively).

Table 1 Seasonal Variations of Physical and Biochemical Characteristics, expressed as Mean ± SD.

Stream size	Season	Month	Water Temperature (°C)	pH	Alkalinity ($\mu mol\ L^{-1}$)	DOC ($mg\ L^{-1}$)
small	Dry	January	14.3 ± 4.1	7.05 ± 0.31	883 ± 548	1.07 ± 0.37
	Wet	April	19.9 ± 1.9	7.19 ± 0.26	615 ± 262	1.51 ± 0.58
	Wet	July	25.7 ± 2.3	7.17 ± 0.27	676 ± 227	1.59 ± 0.97
	Wet	August	27.1 ± 3.0	7.13 ± 0.38	678 ± 308	1.51 ± 0.56
	Dry	October	21.5 ± 2.6	7.08 ± 0.23	778 ± 358	1.16 ± 0.82
large	Dry	January	16.9 ± 5.5	7.00 ± 0.27	961 ± 409	1.70 ± 1.52
	Wet	April	22.1 ± 3.7	7.20 ± 0.27	890 ± 386	2.22 ± 1.65
	Wet	July	27.8 ± 2.9	6.92 ± 0.25	740 ± 305	1.97 ± 1.77
	Wet	August	28.9 ± 3.3	6.92 ± 0.26	739 ± 312	2.47 ± 2.04
	Dry	October	25.2 ± 3.1	7.13 ± 0.29	887 ± 331	1.37 ± 0.67

3.2 Spatial and Seasonal variations in pCO$_2$

The pCO$_2$ ranged from 15 to 6323 µatm with a catchment-wide average of 1748 µatm and showed considerable temporal and spatial variations throughout the sampling period. There was an increasing trend of observed pCO$_2$ from small to large rivers (Figure 3a). On average, the pCO$_2$ values were 856 ± 444, 1481 ± 979, 1354 ± 753, 2332 ± 1330, 2142 ± 1016, 2271 ± 1121, and 2168 ± 1046 µatm for streams from first to seventh order, respectively. The stronger increase in pCO$_2$ occurred between third and fourth order streams (from 1354 ± 753 to 2332 ± 1330 µatm, Figure 3a). Overall, pCO$_2$ in large rivers (2250 ± 1178 µatm) was 76.3 % higher than that in small rivers (1276 ± 796 µatm). Meanwhile, there was also an increasing trend of pCO$_2$ from rivers in the UDJRB compared with those in the LDJRB. The pCO$_2$ values were 2105 ± 959 and 2487 ± 1276 µatm for small and large rivers, respectively, in the LDJRB, which were 146.7% and 70% higher than that in the UDJRB, respectively (Figure 3b).
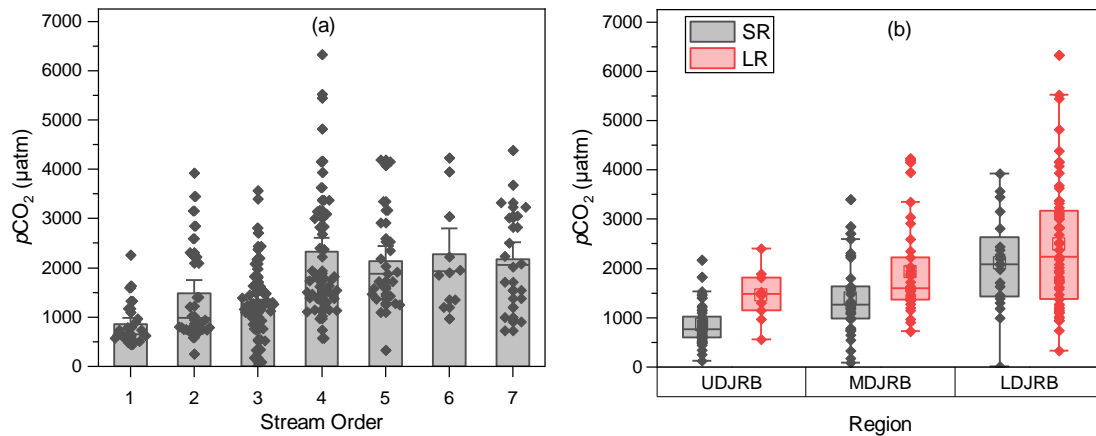
Figure 3 Spatial variations in pCO_2. (a) Yearly average pCO_2 in the seven stream orders, standard errors (SE) are
displayed by error bars. (b) Measured pCO_2 in small and large rivers among three regions in the DJRB. The box
mid-lines represent medians; the interquartile range (IQR) is represented by top and bottom of the box,
respectively; whiskers indicate the range of 1.5 IQR; the white square symbols represent means, and the other
symbols represent pCO_2 values for each sampled site.

Seasonal variations of pCO_2 differed across the stream size spectrum (Figure 4). In small rivers, the
highest pCO_2 was observed in April (1506 ± 880 μatm), which was 50.3 % higher compared with January
(1002 ± 660 μatm). pCO_2 then decreased in July (1131 ± 589 μatm) and increased in August (1325 ± 863
μatm) and October (1414 ± 900 μatm). Compared with small rivers, the peak of pCO_2 in large rivers
occurred later but persisted for a longer period of time. In large rivers, an increase in pCO_2 was not
observed until July. pCO_2 in April was 1831 ± 793 μatm, which was similar to 1805 ± 1010 μatm in
January, and it increased 39.3 % to 2550 ± 1210 μatm in July. pCO_2 peaked in August (2885 ± 1351
μatm) and then decreased to 2176 ± 1166 in October. Overall, pCO_2 was 9.3 % and 21.7 % higher in the
wet season than in the dry season for small and large rivers, respectively.
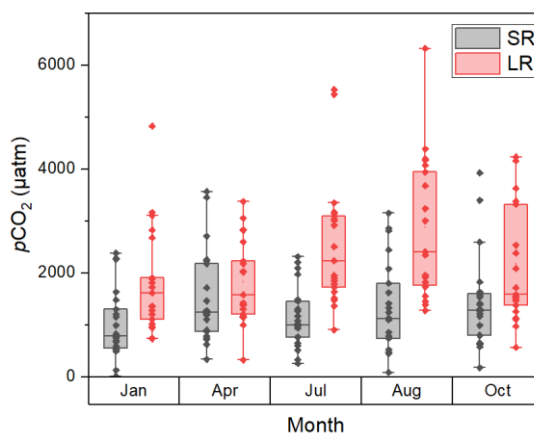
Figure 4 Seasonal pCO_2 changes in small and large rivers. The box mid-lines represent medians; the interquartile range (IQR) is represented by top and bottom of the box, respectively; whiskers indicate the range of 1.5 IQR; the white square symbols represent means, and the other symbols represent pCO_2 values for each sampled site.

3.3 CO$_2$ effluxes and k_{600}

CO$_2$ effluxes ranged from -129.8 to 3874.8 mmol m^{-2} d^{-1} with a mean of 225.2 mmol m^{-2} d^{-1}. More than 95 % of the 196 samples had positive FCO$_2$ values, indicating that a majority of the surveyed rivers is a carbon source. Overall, we observed higher FCO$_2$ during wet season than during dry season in both small and large rivers (Figure 5a). FCO$_2$ in small rivers and large rivers were 264.2 ± 410.0 and 300.1 ± 511.7 mmol m^{-2} d^{-1}, respectively, during the wet season, which was 87.2 % and 123.1 % higher than that in the dry season (141.1 ± 188.7 and 134.5 ± 129.5 mmol m^{-2} d^{-1} for small and large rivers, respectively). No significant (independent sample t test, $p > 0.05$) difference in FCO$_2$ was observed between small and large rivers.

k_{600} differed greatly between river size classes and among hydrological periods (Figure 5b). k_{600} values in small rivers were on average significantly (independent sample t test, $p < 0.001$) higher than that in large rivers. The mean values of k_{600} in small rivers were 8.29 ± 11.29 m d^{-1} and 4.90 ± 3.82 m d^{-1} for the wet season and dry season, respectively, which were 112.6 % and 70 % higher than that of large rivers (3.90 ± 5.55 m d^{-1} in the wet season and 2.25 ± 1.61 m d^{-1} in the dry season). k_{600} during the wet season were also significantly (independent sample t test, $p < 0.05$) higher than that in the dry season. k_{600} increased 112.7 % and 118.2 % from dry season to wet season in small and large rivers, respectively.

However, comparisons between different phases in the same hydrological period (e.g., early, middle, and late wet season) did not differ significantly (paired sample t test, $p > 0.05$) for both river size classes.

280 The spatial and temporal variations of CO_2 efflux generally coincided with the changes in pCO_2 and k_{600}. In small rivers, the highest CO_2 effluxes were 346.8 ± 625.2 mmol m^{-2} d^{-1} during April, consistent with the high k_{600} and pCO_2 in this period. In large rivers, high CO_2 effluxes were observed in both April (339.9 ± 828.6 mmol m^{-2} d^{-1}) and August (329.9 ± 270.0 mmol m^{-2} d^{-1}), which were attributed to the concurrently high k_{600} in April and high pCO_2.
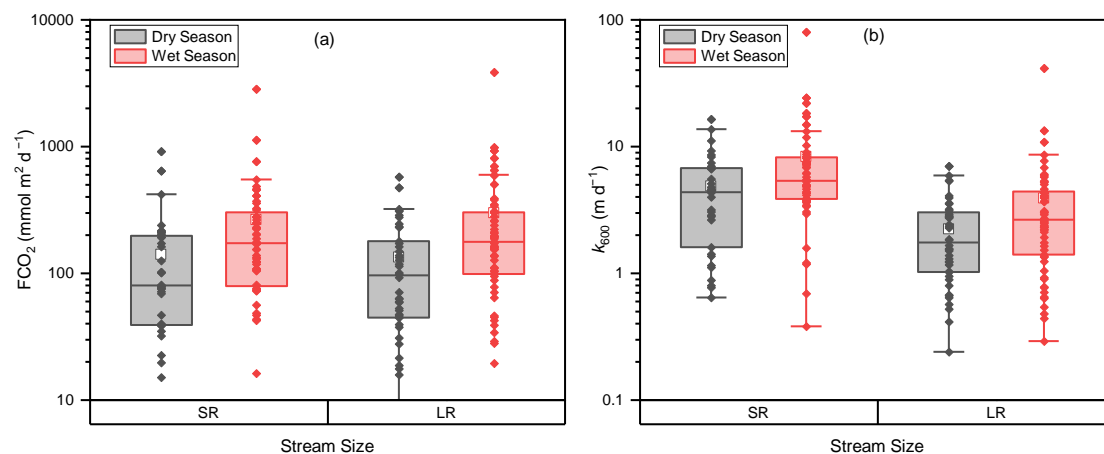
285

Figure 5 Relationship between stream size and (a) FCO$_2$ and (b) k_{600}. The box mid-lines represent medians; the interquartile range (IQR) is represented by top and bottom of the box, respectively; whiskers indicate the range of 1.5 IQR; the white square symbols represent means, and the other symbols represent FCO$_2$ and k_{600} values for each sampled site.

290 **4 Discussions**

4.1 Underlying Processes of pCO$_2$ dynamics

The spatial pattern of pCO_2 in the DJRB is likely resulting from the changes in terrestrial carbon inputs (i.e., organic and inorganic carbon) and in-stream metabolism, both of which varied due to different land cover and catchment topography. The higher pCO_2 values in large rivers than small rivers were

295 associated with a higher percentage of urban and cropland cover and a lower forest cover (Figure 6). Compared with forest, cropland could provide a more favourable condition for soil erosion and the transfer of terrestrial carbon from land to rivers, contributing to a higher pCO_2. Intensification of

agricultural practices could promote the decomposition of soil organic matter (Borges et al., 2018), thereby increasing the concentration of CO_2 and liable DOC in the soil (Borges et al., 2018). The soil CO_2 could be easily transported to rivers and thus increase the pCO_2, while the liable DOC could be decomposed rapidly after entering the rivers due to their sensitivity to in-stream metabolism (Lambert et al., 2017; Li et al., 2019). Meanwhile, the input of wastewater with high organic matter concentration from urban areas could also contribute to an increase in riverine pCO_2 (Xuan et al., 2020; Zhang et al., 2021). Our results showed increasing pCO_2 from forest-dominated streams in the UDJRB relative to those in agricultural and urban impacted catchments in the MDJRB and LDJRB (Figure 3b). The >70% forest cover in the UDJRB (Figure 1) may have greatly reduced the soil erosion intensity (Ran et al., 2018). Meanwhile, the organic matter from forest tends to be more aromatic, thus more capable of surviving biodegradation (Kalbitz and Kaiser, 2008), leading to a relatively low riverine pCO_2 value. In contrast, cropland, occupying about 49% of the land cover (Figure 1), was the primary land use type in the MDJRB substituting forest, and urban areas account for ~17% of the land cover in the LDJRB. The higher pCO_2 in the MDJRB and LDJRB is likely under the influence of agricultural practices and wastewater input. Overall, land use mainly affects the spatial distribution of pCO_2 by altering the amount and lability of carbon inputs to the rivers.
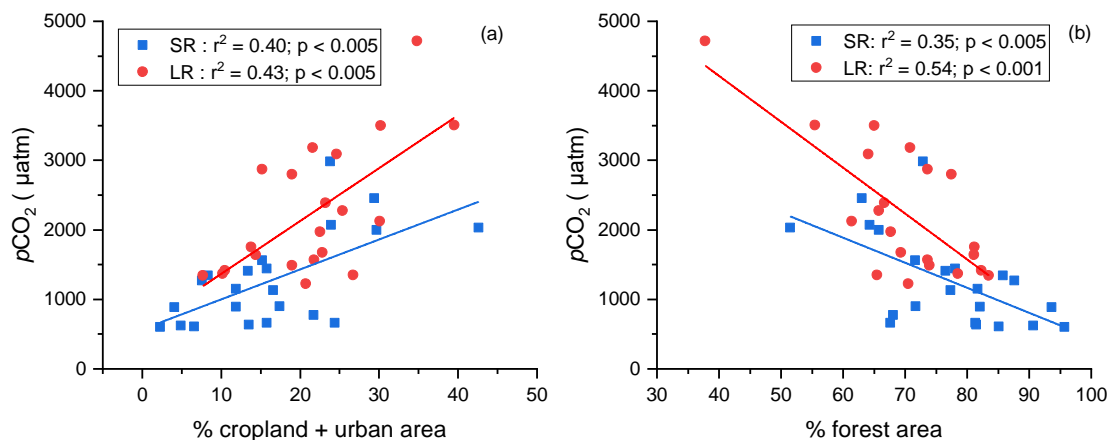
Figure 6 (a) the relationship between yearly average pCO_2 at each site and the percentage of cropland and urban area combined, (b) the relationship between yearly average pCO_2 at each site and the percentage of forest area

Moreover, different catchment topography in small and large rivers may have also contributed to the differences in pCO$_2$. Due to steeper channel slopes and higher flow velocities, small rivers in the DJRB

320   have higher k600 (Figure 5b). As a consequence, CO$_2$ in small rivers can exchange with the atmosphere more rapidly, preventing the build-up of dissolved CO$_2$ and thus lower pCO$_2$ (Rocher-Ros et al., 2019). Therefore, other processes have facilitated the carbon transfer from small rivers to downstream large rivers, sustaining the higher pCO$_2$ in large rivers. Recent studies indicate that carbonate buffering could decrease the CO$_2$ emissions from small rivers by increasing the ionization of CO$_2$ (Stets et al., 2017),

325   thereby increasing the transfer of DIC towards the rivers downstream, which resulted in the higher pCO$_2$ in downstream large rivers . However, strong carbonate buffering usually occurs in high-alkalinity (>2500 μmol L^{-1}) streams with high pH (>8), while in low-alkalinity waters, the pool of ionized CO$_2$ is relatively small, indicating a weak carbonate buffering (Stets et al., 2017). Since the streams in the DJRB were characterized by low alkalinity (726 ± 364 μmol L^{-1} and 844 ± 409 μmol L^{-1} for small and large

330   rivers, respectively), carbonate buffering is unlikely a primary contributor to the high pCO$_2$ in large rivers. Meanwhile, our data showed that river water pCO$_2$ was negatively related to DO and positively related to DOC (Figure 7), suggesting that the high pCO$_2$ in large river was related to metabolic processes. The steep channel slopes in small rivers tend to promote the transfer of OC to downstream large rivers. As a consequence, it is difficult for terrestrial organic carbon to be converted into CO$_2$ in small rivers due to

335   the short water residence time (Hotchkiss et al., 2015). Conversely, a greater fraction of OC may have been transported downstream and fuel the heterotrophic respiration in large rivers, where low flow velocity and long water residence time facilitated the decomposition of organic carbon within the water column (Denfeld et al., 2013).
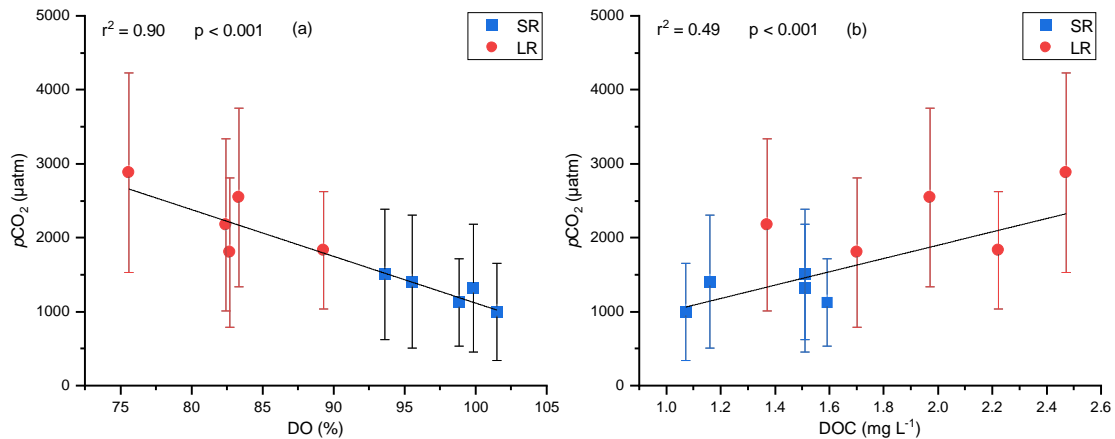
Figure 7 Relationship between seasonal average pCO_2 and (a) DO and (b) DOC. Error bars for the pCO_2 represent 1 standard deviation from the seasonal mean. The DO–pCO_2 and DOC–pCO_2 relationship are shown as solid lines.

To compare the contribution of internal metabolism and external CO_2 input on pCO_2 in small and large rivers, the ΔCO_2:ΔO_2 stoichiometry was used to evaluate the impacts of respiration and photosynthesis processes on the concentration of dissolved O_2 and CO_2 (Stets et al., 2017). The inverse relation between ΔCO_2 and ΔO_2 (Figure 8) demonstrated that metabolic processes are important for the dissolved CO_2 concentration variations (Amaral et al., 2020), while the difference in the ΔCO_2:ΔO_2 stoichiometry between small and large rivers suggested the different strength of in-stream metabolism (Rasera et al., 2013). The ΔCO_2:ΔO_2 stoichiometry in large rivers is closer to the 1:1 line than that in small rivers, indicating that large rivers are more affected by the metabolic processes (Jeffrey et al., 2018; Amaral et al., 2020). For large rivers, the linear regression is $\Delta CO_2 = -0.999\ (\pm\ 0.081)\ \Delta O_2 + 18.020\ (\pm\ 5.995)$ ($r^2 = 0.62$, $p < 0.001$). When the CO_2 concentration increases in large rivers, a similar magnitude of decrease in dissolved O_2 concentration occurs, indicating that in-stream metabolism is the primary control on pCO_2. In contrast, the linear regression for small rivers is $\Delta CO_2 = -0.868\ (\pm\ 0.098)\ \Delta O_2 + 21.42\ (\pm 4.175)$ ($r^2 = 0.41$, $p < 0.001$), which means that with the CO_2 concentration increasing by 1 µmol L^{-1}, the O_2 concentration decreases by only 0.868 µmol L^{-1}. Therefore, extra CO_2 inputs have contributed to the changes in pCO_2 despite the strong presence of in-stream metabolism.
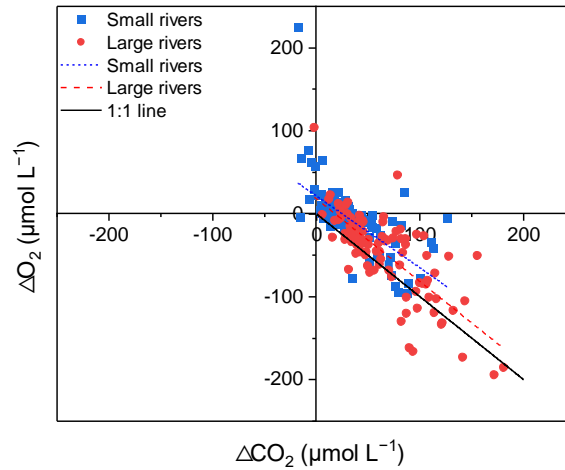
Figure 8 The relationship between ΔCO_2 and ΔO_2. Points greater than zero are oversaturated, and less than zero are undersaturated. Points above the 1:1 line indicate the existence of additional carbon sources, apart from in-stream metabolic processes. For large rivers, the linear regression is $\Delta CO_2 = -0.999\ (\pm 0.081)\ \Delta O_2 +18.020\ (\pm 5.995)$ ($r^2 = 0.62$, $p < 0.001$). For small rivers, the linear regression is $\Delta CO_2 = -0.868\ (\pm 0.098)\ \Delta O_2 + 21.42\ (\pm 4.175)$ ($r^2 = 0.41$, $p < 0.001$).

On the other hand, the temporal pattern was affected by precipitation and temperature seasonality. Our results showed that higher pCO_2 occurred in the wet season than in the dry season for both small and large rivers (Figure 4). The elevated temperature in the wet season could promote a substantial increase in the net primary productivity of the terrestrial ecosystem, while increased precipitation can facilitate the transfer of terrestrial carbon (Rasera et al., 2013), including both soil CO_2 and OC, from land to rivers. This could either directly increase riverine pCO_2, or fuel OC decomposition (Borges et al., 2018). However, the differences in seasonal changes of pCO_2 between small and large rivers (Figure 4) also suggested that their controlling process could be different. For small rivers, the highest pCO_2 value was observed in April (Figure 4), which is consistent with the rapid surge of terrestrial C inputs, usually occurring at the onset of the wet season (Hope et al., 2004; Yao et al., 2007; Johnson et al., 2008). However, such increase in pCO_2 was not observed in large rivers (Figure 4) though the DOC in large rivers increased at a rate similar to that in small rivers during the same period (Table 1). A possible explanation is that the observed pCO_2 rise was mainly originated from soil CO_2, which was readily emitted from the small rivers into the air, with little reaching the larger rivers downstream (Denfeld et al., 2013; Drake et al., 2018). Differences in the pCO_2 dynamics in July and August also reflected different controlling processes in small and large rivers. A decline in pCO_2 in July in small rivers

suggested that it might have experienced the depletion effect occurring in the middle and late wet season
(Hope et al., 2004), during which soil CO_2 decreased due to the continual precipitation. In contrast, the increase in pCO_2 in large rivers in July indicated that the decreased soil CO_2 inputs could hardly affect the pCO_2 in large rivers during this period. Instead, stronger in-stream metabolism caused by OC inputs and the favourable conditions for OC decomposition are more likely to be responsible for the rising pCO_2. In addition, there are other processes that may have affected the riverine pCO_2. For example, stronger solar radiation during summer could increase photo-oxidation in rivers. However, the commonly observed lower daytime CO_2 emission rates than nocturnal rates (Gómez-Gener et al., 2021) suggest that photosynthesis overrides photo-oxidation in CO_2 dynamics. Nonetheless, the low DO concentration observed in the surveyed rivers (Figure 8) suggested that photosynthesis is not likely the primary control on the seasonal variation of pCO_2.

4.2 Environmental Control of k_{600} variation

Environmental factors, including wind speed and hydrological variables, could affect the gas exchange at the water–air interface and are typically used to explain the variance in k_{600} (Alin et al., 2011; Raymond et al., 2012). Flow velocity generally determines the k_{600} in small rivers, while wind speed becomes a more important factor in controlling the k_{600} in large rivers, reservoirs, and estuary (Guérin et al., 2007; Rasera et al., 2013; Amaral et al., 2020). In our surveyed rivers, k_{600} displayed a significant linear correlation (Pearson correlation, $p < 0.001$) with the flow velocity. Our k_{600} model (Figure 9) based on 188 field measurement data is similar to that developed by Alin et al. (2011) ($k_{600} = 13.82 + 0.35v$). However, in our studied rivers, no significant correlation (Pearson correlation,$p > 0.05$) was found between wind speed and k_{600} regardless of stream size. This could be explained by the lower wind speed (0.68 ± 0.66 m s^{-1} and 1.09 ± 1.06 m s^{-1} for small and large rivers, respectively; Table 2) (Guérin et al., 2007). As the wind speed decreases, the impact of flow velocity on k_{600} becomes increasingly predominant (Borges et al., 2004). Therefore, the accuracy of k_{600} estimation based on wind speed in nearby regions should be examined using measurement data (Yao et al., 2007; Li et al., 2018). The temporal heterogeneities of k_{600} between small and large rivers reveal the differences in flow regime. The k_{600} in small rivers are significantly higher than that in large rivers (independent sample t test, $p < 0.001$), which could be explained by the higher flow velocity in small rivers. Meanwhile, the significantly higher k_{600} in the wet season than in the dry season (independent sample t test, $p < 0.05$) is the result of the

increased flow velocity and turbulence due to monsoon-induced precipitation during the wet season (Guérin et al., 2007; Alin et al., 2011; Ho et al., 2018).
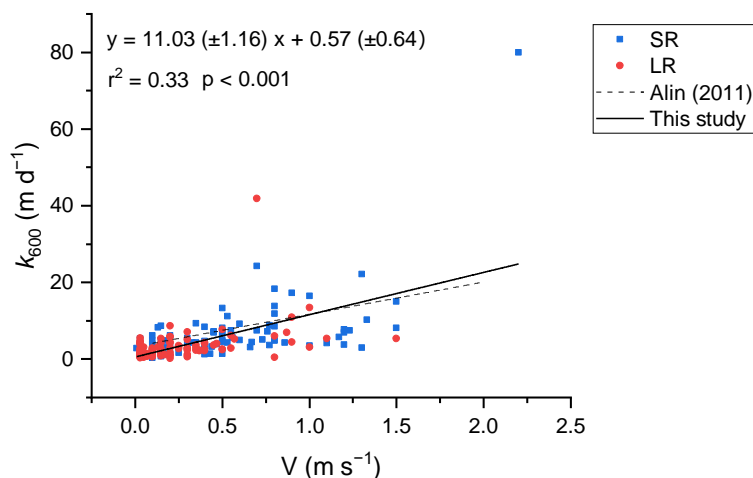
Figure 9 Relationship between k_{600} and flow velocity. The dashed line represents the parameterization of Alin et al (2011).

Table 2. Seasonal variation of k_{600} and environmental factors in small and large rivers.

Stream size	Season	Current velocity (m s^{-1})	U10 (m s^{-1})	k_{600} (m d^{-1})
small	Wet	0.66 ± 0.47	0.62 ± 0.61	8.29 ± 11.29
	Dry	0.43 ± 0.27	0.76 ± 0.73	4.90 ± 3.82
large	Wet	0.32 ± 0.32	0.86 ± 0.91	3.90 ± 5.55
	Dry	0.17 ± 0.19	1.43 ± 1.58	2.25 ± 1.61

Exceptionally high k_{600} values were observed in the surveyed rivers (Figure 9). The highest k_{600} in large and small rivers were 41.83 and 79.97 m d^{-1}, respectively, which were 5-fold and 3-fold larger than calculated k_{600}, respectively. This is likely the result of the exponential increase in k_{600} due to extreme flood events. Generally, flood events associated with heavy rainfall can substantially increase flow velocity and near-surface turbulence (Almeida et al., 2017; Geeraert et al., 2017), leading to extremely high k_{600} values. Yet, neither our model nor the one from Alin et al. (2011) was suitable for the estimation of k_{600} during extreme flood events because the calculated k_{600} could deviate far from the measured k_{600} when they occurred. The extent to which flood events affect k_{600} and riverine CO_2 emission is still uncertain and warrant continued research (Drake et al., 2018).

4.3 A Comparison of CO_2 Emissions to Other Rivers

The mean CO_2 fluxes of 225.2 mmol $m^{-2} d^{-1}$ in the DJRB is comparable to those observed in tropical
425   and subtropical rivers in the Americas, Africa, and Southeast Asia (Table 3). Although the magnitude
of the CO_2 emissions of these river systems is similar, the seasonal variations and drivers behind them
could differ. The CO_2 emissions from the Dongjiang River were higher in the wet season than in the dry
season. This seasonal pattern is similar to that observed in the Xijiang and Daning rivers (Yao et al.,
2007; Ni et al., 2019) but different from that observed in the Jinshui River in the upper Yangtze River,
430   where pCO_2 is high in winter and low in summer (Luo et al., 2019), although all four rivers are in the
East Asia Monsoon climate region. The seasonal differences in CO_2 emissions are largely caused by the
pCO_2 variability, which in turn is regulated by external carbon inputs, internal production of CO_2 (Yao
et al., 2007), and the dilution effect caused by precipitation (Johnson et al., 2007). For rivers where pCO_2
is lower in summer than in winter, the dilution effect overrides the effect of increased carbon inputs and
435   internal CO_2 production (Luo et al., 2019). In contrast, for rivers like the Dongjiang River, although the
dilution effect remains, increased CO_2 inputs and metabolism are more significant factors in controlling
its pCO_2, thus leading to higher summer pCO_2. In addition, the controlling processes of the Dongjiang
River could be different even when compared with rivers with similar seasonal variations in the same
climatic zone. For instance, the DO in the Xijiang river was supersaturated, indicating that its aquatic
440   photosynthetic activities predominated aquatic metabolism and tended to reduce its CO_2 concentration
(Yao et al., 2007). Therefore, other carbon sources like soil respiration and carbonate weathering should
be responsible for the high pCO_2 in summer (Zhang et al., 2019). In contrast, the low DO value and the
negative correlation between DO and pCO_2 in the Dongjiang River indicated that photosynthesis is
relatively weak compared with the respiration, and the latter process is an essential source of riverine
445   CO_2 (Stets et al., 2017), resulting in a higher pCO_2 in summer.

Table 3. Comparison of CO_2 emissions from subtropical and tropical rivers.

Rivers	Climate	Season	pCO_2 (µatm)	k_{600} (m d^{-1})	FCO_2 (mmol m^{-2} d^{-1})	References
The Dongjiang River (Large rivers)	Subtropical	Wet	2422 ± 1209	3.90 ± 5.55	300.1 ± 511.8	This study
		Dry	1990 ± 1094	2.25 ± 1.61	134.5 ± 129.5	
The Dongjiang River (small rivers)		Wet	1321 ± 792	8.29 ± 11.29	264.2 ± 410.0	
		Dry	1191 ± 825	4.90 ± 3.82	129.5 ± 197.2	
The Xijiang River (Mainstream)	Subtropical		2600		190.3–358.6	(Yao et al., 2007)
The Lower Mekong River	Tropical		1090 ± 290	6.24*	194.5	(Li et al., 2013)
The Yangtze River (Jinshui River) (headwater stream)	Subtropical		1147 ± 874	11.1 ± 4.5*	343 ± 413	(Luo et al., 2019)
		Dry	1562 ± 975		542 ± 477	
		Wet	834 ± 639		192 ± 278	
The upper Yangtze River (Daning river)	Subtropical		1198.2 ± 1122.9		329.8 ± 470.2	(Ni et al., 2019)
		Rainy	1243.7 ± 1111.5	8.1–14.1*	357.4 ± 483.7	
		Dry	1145.5 ± 1146.2	7.0–8.8*	288.7 ± 450.0	
The Zambezi River	Tropical	Wet	3102.5 **	0.05–1.51	350.75	(Teodoru et al., 2014)
		Dry	1150 **		51.92	
The Congo River	Tropical	High water	6001 ± 5008		1149 or 1520	(Borges et al., 2015a; Borges et al., 2015b)
		Low water	4867 ± 2578			
		Falling water	5321 ± 3383			
The Lower Red River	Tropical		1589 ± 43	12.22 ± 6.48	530.3 ± 16.9	(Le et al., 2018)
Caboolture River	Subtropical		3000 ± 33		379 ± 53	(Jeffrey et al., 2018)
Rajang River	Tropical	wet	2531 ± 188	0.55–2.93	141.67	(Müller-Dum et al., 2019)
		dry	2337 ± 304		125	
Lower Mississippi River	Subtropical		1514 ± 652		172.8	(Reiman and Xu, 2019b)
Amazonian Rivers	Tropical		259–7808	5.06	69.12–1321.92	(Rasera et al., 2013)

* k values wereshown here because k_{600} values were not provided in references; ** the unit for pCO_2 is ppm.

450 The CO_2 fluxes in small rivers are similar to those in large rivers, which is contradictory to the finding in previous studies that CO_2 effluxes should be higher in small rivers than in large rivers due to the input of CO_2-rich groundwater (Duvert et al., 2018). The depletion and diffusion effect may be responsible for the discrepancy (Johnson et al., 2007; Dinsmore et al., 2013). Groundwater in the DJRB could be easily diluted due to abundant monsoon-induced rainfall, preventing it from supplying the small rivers with

455 high CO_2 concentrations. However, we recognize that the impact of groundwater on pCO$_2$ in small rivers may be overlooked in our sampling process since the CO_2 carried by groundwater can emit into the atmosphere within a very short distance (Duvert et al., 2018). In view of the above, it is recommended that further studies targeting the release of groundwater CO_2 to the atmosphere be carried out in the future.

5 Conclusion

460 Studying CO_2 emissions from subtropical rivers is an essential step toward more accurate estimates of global CO_2 emissions from river systems. By deploying floating chambers, seasonal changes in riverine pCO$_2$ and CO_2 emissions from the Dongjiang River catchment were investigated. Spatial and temporal patterns of pCO$_2$ were mainly affected by terrestrial carbon inputs (i.e., organic and inorganic carbon) and in-stream metabolism, both of which varied due to different land cover, catchment topography, and

465 seasonality of precipitation and temperature. k_{600} was higher in small rivers than in large rivers and higher during the wet season than during the dry season, both of which can be explained by the observed significant correlation between k_{600} and flow velocity. In contrast to previous studies, similar CO_2 fluxes were observed among small and large rivers in the DJRB. It is suggested that the absence of commonly observed higher CO_2 fluxes in small rivers could be associated with the depletion effect caused by

470 abundant and persistent precipitation in this subtropical monsoon catchment. There is no doubt that the spatial and temporal variations of CO_2 emissions from the DJRB reflected the complexity and diversity of controlling factors. As a step towards a more accurate estimate of the carbon budget in the catchment, comprehensive and systematic measurements of CO_2 emissions covering a broad range of stream sizes and seasons are of paramount importance.

475 *Data availability.* CO_2 emission data used in this study are available online at: https://doi.org/ 10.25442/hku.13416281.v1 (Liu, 2020). Other data are available from the corresponding author Lishan Ran upon request at lsran@hku.hk.

Author contributions. BL and LR conceived the study. BL, MT, CC, XY, and LR carried out the fieldwork. BL, MT, and KS designed and performed the laboratory analysis. BL composed the manuscript with contributions from all authors.

Competing interests. The authors declare that they have no conflict of interest.

Acknowledgements. This work was financially supported by the Research Grants Council of Hong Kong (Grants: 17300619 and 27300118), the Hui Oi-Chow Trust Fund (Grant: 201801172006) and the National Natural Science Foundation of China (Grant: 41807318). We thank Dr Steven Bouillon and the two anonymous reviewers for their constructive comments which have greatly improved the manuscript.

References

Abril, G., Martinez, J. M., Artigas, L. F., Moreira-Turcq, P., Benedetti, M. F., Vidal, L., Meziane, T., Kim, J. H., Bernardes, M. C., Savoye, N., Deborde, J., Souza, E. L., Alberic, P., Landim de Souza, M. F., and Roland, F.: Amazon River carbon dioxide outgassing fuelled by wetlands, Nature, 505, 395-398, https://doi.org/10.1038/nature12797, 2014.

Abril, G., Bouillon, S., Darchambeau, F., Teodoru, C. R., Marwick, T. R., Tamooh, F., Ochieng Omengo, F., Geeraert, N., Deirmendjian, L., Polsenaere, P., and Borges, A. V.: Technical Note: Large overestimation of pCO_2 calculated from pH and alkalinity in acidic, organic-rich freshwaters, Biogeosciences, 12, 67-78, https://doi.org/10.5194/bg-12-67-201510.5194, 2015.

Alin, S. R., Rasera, M. d. F. F. L., Salimon, C. I., Richey, J. E., Holtgrieve, G. W., Krusche, A. V., and Snidvongs, A.: Physical controls on carbon dioxide transfer velocity and flux in low-gradient river systems and implications for regional carbon budgets, Journal of Geophysical Research, 116, G01009, https://doi.org/10.1029/2010jg001398, 2011.

Almeida, R. M., Pacheco, F. S., Barros, N., Rosi, E., and Roland, F.: Extreme floods increase CO_2 outgassing from a large Amazonian river, Limnology and Oceanography, 62, 989-999, https://doi.org/10.1002/lno.10480, 2017.

Amaral, J. H. F., Melack, J. M., Barbosa, P. M., MacIntyre, S., Kasper, D., Cortés, A., Silva, T. S. F., Nunes de Sousa, R., and Forsberg, B. R.: Carbon dioxide fluxes to the atmosphere from waters within flooded forests in the Amazon basin, Journal of Geophysical Research: Biogeosciences, 125, e2019JG005293, https://doi.org/10.1029/2019JG005293, 2020.

Battin, T. J., Luyssaert, S., Kaplan, L. A., Aufdenkampe, A. K., Richter, A., and Tranvik, L. J.: The boundless carbon cycle, Nature Geoscience, 2, 598-600, https://doi.org/10.1038/ngeo618, 2009.

Borges, A. V., Delille, B., Schiettecatte, L. S., Gazeau, F., Abril, G., Frankignoulle, M. J. L., and Oceanography: Gas transfer velocities of CO_2 in three European estuaries (Randers Fjord, Scheldt, and Thames), Limnology Oceanography, 49, 1630-1641, https://doi.org/10.4319/lo.2004.49.5.1630, 2004.

Borges, A. V., Abril, G., Darchambeau, F., Teodoru, C. R., Deborde, J., Vidal, L. O., Lambert, T., and Bouillon, S.: Divergent biophysical controls of aquatic CO2 and CH4 in the World's two largest rivers, Scientific Reports, 5, 15614, 10.1038/srep15614, 2015a.

Borges, A. V., Darchambeau, F., Teodoru, C. R., Marwick, T. R., Tamooh, F., Geeraert, N., Omengo, F. O., Guérin, F., Lambert, T., Morana, C., Okuku, E., and Bouillon, S.: Globally significant greenhouse-gas emissions from African inland waters, Nature Geoscience, 8, 637-642, 10.1038/ngeo2486, 2015b.

Borges, A. V., Darchambeau, F., Lambert, T., Bouillon, S., Morana, C., Brouyere, S., Hakoun, V., Jurado, A., Tseng, H. C., Descy, J. P., and Roland, F. A. E.: Effects of agricultural land use on fluvial carbon dioxide, methane and nitrous oxide concentrations in a large European river, the Meuse (Belgium), Science of The Total Environment, 610-611, 342-355, https://doi.org/10.1016/j.scitotenv.2017.08.047, 2018.

Chen, Q., Xu, W., Li, S., Fu, S., and Yan, J.: Aboveground biomass and corresponding carbon sequestration ability of four major forest types in south China, Chinese Science Bulletin, 58, 1551-1557, 10.1007/s11434-012-5100-8, 2013.

Chen, Y. D., Zhang, Q., Lu, X., Zhang, S., and Zhang, Z.: Precipitation variability (1956–2002) in the Dongjiang River (Zhujiang River basin, China) and associated large-scale circulation, Quaternary International, 244, 130-137, https://doi.org/10.1016/j.quaint.2010.08.013, 2011.

Cole, J. J., Prairie, Y. T., Caraco, N. F., McDowell, W. H., Tranvik, L. J., Striegl, R. G., Duarte, C. M., Kortelainen, P., Downing, J. A., Middelburg, J. J., and Melack, J.: Plumbing the global carbon cycle: Integrating inland waters into the terrestrial carbon budget, Ecosystems, 10, 172-185,

https://doi.org/10.1007/s10021-006-9013-8, 2007.

Dean, J. F., Garnett, M. H., Spyrakos, E., and Billett, M. F.: The potential hidden age of dissolved organic carbon exported by peatland streams, Journal of Geophysical Research: Biogeosciences, 124, 328-341, 535   2019.

Denfeld, B. A., Frey, K. E., Sobczak, W. V., Mann, P. J., and Holmes, R. M.: Summer CO_2 evasion from streams and rivers in the Kolyma River basin, north-east Siberia, Polar Research, 32, 19704, https://doi.org/10.3402/polar.v32i0.19704, 2013.

Dickson, A. G., Sabine, C. L., and Christian, J. R.: Guide to best practices for ocean CO_2 measurements, 540   North Pacific Marine Science Organization, 2007.

Ding, J., Jiang, Y., Fu, L., Liu, Q., Peng, Q., and Kang, M.: Impacts of land use on surface water quality in a subtropical river basin: A case study of the Dongjiang River Basin, Southeastern China, Water, 7, 4427-4445, https://doi.org/10.3390/w7084427, 2015.

Dinsmore, K. J., Wallin, M. B., Johnson, M. S., Billett, M. F., Bishop, K., Pumpanen, J., and Ojala, A.: 545   Contrasting CO_2 concentration discharge dynamics in headwater streams: A multi-catchment comparison, Journal of Geophysical Research: Biogeosciences, 118, 445-461, https://doi.org/10.1002/jgrg.20047, 2013.

Drake, T. W., Raymond, P. A., and Spencer, R. G.: Terrestrial carbon inputs to inland waters: A current synthesis of estimates and uncertainty, Limnology and Oceanography Letters, 3, 132-142, 550   https://doi.org/10.1002/lol2.10055, 2018.

Duvert, C., Butman, D. E., Marx, A., Ribolzi, O., and Hutley, L. B.: CO_2 evasion along streams driven by groundwater inputs and geomorphic controls, Nature Geoscience, 11, 813-818, https://doi.org/10.1038/s41561-018-0245-y, 2018.

Fu, Y., Tang, C., Li, J., Zhao, Y., Zhong, W., and Zeng, X.: Sources and transport of organic carbon from 555   the Dongjiang River to the Humen outlet of the Pearl River, southern China, Journal of Geographical Sciences, 24, 143-158, https://doi.org/10.1007/s11442-014-1078-2, 2014.

Geeraert, N., Omengo, F. O., Borges, A. V., Govers, G., and Bouillon, S.: Shifts in the carbon dynamics in a tropical lowland river system (Tana River, Kenya) during flooded and non-flooded conditions, Biogeochemistry, 132, 141-163, https://doi.org/10.1007/s10533-017-0292-2, 2017.

560   Gómez-Gener, L., Rocher-Ros, G., Battin, T., Cohen, M. J., Dalmagro, H. J., Dinsmore, K. J., Drake, T. W., Duvert, C., Enrich-Prast, A., Horgby, Å., Johnson, M. S., Kirk, L., Machado-Silva, F., Marzolf, N. S., McDowell, M. J., McDowell, W. H., Miettinen, H., Ojala, A. K., Peter, H., Pumpanen, J., Ran, L., Riveros-Iregui, D. A., Santos, I. R., Six, J., Stanley, E. H., Wallin, M. B., White, S. A., and Sponseller, R. A.: Global carbon dioxide efflux from rivers enhanced by high nocturnal emissions, Nature 565   Geoscience, 10.1038/s41561-021-00722-3, 2021.

Guérin, F., Abril, G., Serça, D., Delon, C., Richard, S., Delmas, R., Tremblay, A., and Varfalvy, L.: Gas transfer velocities of CO_2 and CH_4 in a tropical reservoir and its river downstream, Journal of Marine Systems, 66, 161-172, https://doi.org/10.1016/j.jmarsys.2006.03.019, 2007.

Ho, D. T., Engel, V. C., Ferrón, S., Hickman, B., Choi, J., and Harvey, J. W.: On factors influencing air‑ 570   water gas exchange in emergent wetlands, Journal of Geophysical Research: Biogeosciences, 123, 178-192, https://doi.org/10.1002/2017JG004299, 2018.

Hope, D., Billett, M., and Cresser, M.: A review of the export of carbon in river water: fluxes and processes, Environmental pollution, 84, 301-324, 1994.

Hope, D., Palmer, S. M., Billett, M. F., and Dawson, J. J. J. H. P.: Variations in dissolved CO_2 and CH_4 575   in a first‑order stream and catchment: an investigation of soil‑stream linkages, Journal of Hydrological Processes, 18, 3255-3275, https://doi.org/10.1002/hyp.5657, 2004.

Hotchkiss, E., Hall Jr, R., Sponseller, R., Butman, D., Klaminder, J., Laudon, H., Rosvall, M., and

Karlsson, J. J. N. G.: Sources of and processes controlling CO_2 emissions change with the size of streams and rivers, Nature Geoscience, 8, 696-699, https://doi.org/10.1038/ngeo2507, 2015.

580   Jeffrey, L. C., Santos, I. R., Tait, D. R., Makings, U., and Maher, D. T.: Seasonal drivers of carbon dioxide dynamics in a hydrologically modified subtropical tidal river and estuary (Caboolture River, Australia), Journal of Geophysical Research: Biogeosciences, 123, 1827-1849, https://doi.org/10.1029/2017jg004023, 2018.

Johnson, M. S., Weiler, M., Couto, E. G., Riha, S. J., and Lehmann, J.: Storm pulses of dissolved CO_2 in
585   a forested headwater Amazonian stream explored using hydrograph separation, Water resources research, 43, https://doi.org/10.1029/2007WR006359, 2007.

Johnson, M. S., Lehmann, J., Riha, S. J., Krusche, A. V., Richey, J. E., Ometto, J. P. H., and Couto, E. G.: CO_2 efflux from Amazonian headwater streams represents a significant fate for deep soil respiration, Geophysical Research Letters, 35, https://doi.org/10.1029/2008GL034619, 2008.

590   Kalbitz, K., and Kaiser, K.: Contribution of dissolved organic matter to carbon storage in forest mineral soils, Journal of Plant Nutrition and Soil Science, 171, 52-60, https://doi.org/10.1002/jpln.200700043, 2008.

Lambert, T., Bouillon, S., Darchambeau, F., Morana, C., Roland, F. A. E., Descy, J.-P., and Borges, A. V.: Effects of human land use on the terrestrial and aquatic sources of fluvial organic matter in a temperate
595   river basin (The Meuse River, Belgium), Biogeochemistry, 136, 191-211, 10.1007/s10533-017-0387-9, 2017.

Lauerwald, R., Laruelle, G. G., Hartmann, J., Ciais, P., and Regnier, P. A.: Spatial patterns in CO_2 evasion from the global river network, Global Biogeochemical Cycles, 29, 534-554, https://doi.org/10.1002/2014GB004941, 2015.

600   Le Coz, J., Pierrefeu, G., and Paquier, A.: Evaluation of river discharges monitored by a fixed side-looking Doppler profiler, Water Resources Research, 44, https://doi.org/10.1029/2008WR006967, 2008.

Le, T. P. Q., Marchand, C., Ho, C. T., Da Le, N., Duong, T. T., Lu, X., Doan, P. K., Nguyen, T. K., Nguyen, T. M. H., and Vu, D. A.: CO_2 partial pressure and CO_2 emission along the lower Red River (Vietnam), Biogeosciences, 15, 4799-4814, https://doi.org/10.5194/bg-15-4799-2018, 2018.

605   Li, S., Lu, X. X., and Bush, R. T.: CO_2 partial pressure and CO_2 emission in the Lower Mekong River, Journal of Hydrology, 504, 40-56, https://doi.org/10.1016/j.jhydrol.2013.09.024, 2013.

Li, S., Ni, M., Mao, R., and Bush, R. T.: Riverine CO_2 supersaturation and outgassing in a subtropical monsoonal mountainous area (Three Gorges Reservoir Region) of China, Journal of Hydrology, 558, 460-469, https://doi.org/10.1016/j.jhydrol.2018.01.057, 2018.

610   Li, X., Xu, J., Shi, Z., and Li, R.: Response of Bacterial Metabolic Activity to the River Discharge in the Pearl River Estuary: Implication for CO2 Degassing Fluxes, Frontiers in Microbiology, 10, 10.3389/fmicb.2019.01026, 2019.

Liang, B., Hu, J. T., Li, S. Y., Ye, Y. X., Liu, D. H., and Huang, J.: Carbon system simulation in the Pearl River Estuary, China: Mass fluxes and transformations, Journal of Geophysical Research:
615   Biogeosciences, 125, e2019JG005012, https://doi.org/10.1029/2019jg005012, 2020.

Luo, J., Li, S., Ni, M., and Zhang, J.: Large spatiotemporal shifts of CO_2 partial pressure and CO_2 degassing in a monsoonal headwater stream, Journal of Hydrology, 579, 124135, https://doi.org/10.1016/j.jhydrol.2019.124135, 2019.

Marx, A., Dusek, J., Jankovec, J., Sanda, M., Vogel, T., van Geldern, R., Hartmann, J., and Barth, J. A.
620   C.: A review of CO_2 and associated carbon dynamics in headwater streams: A global perspective, Reviews of Geophysics, 55, 560-585, https://doi.org/10.1002/2016rg000547, 2017.

Millero, F. J., Graham, T. B., Huang, F., Bustos-Serrano, H., and Pierrot, D.: Dissociation constants of carbonic acid in seawater as a function of salinity and temperature, Marine Chemistry, 100, 80-94,

https://doi.org/10.1016/j.marchem.2005.12.001, 2006.

625   Moramarco, T., Saltalippi, C., and Singh, V. P.: Estimation of Mean Velocity in Natural Channels Based on Chiu’s Velocity Distribution Equation, Journal of Hydrologic Engineering, 9, 42-50, doi:10.1061/(ASCE)1084-0699(2004)9:1(42), 2004.

Müller-Dum, D., Warneke, T., Rixen, T., Müller, M., Baum, A., Christodoulou, A., Oakes, J., Eyre, B. D., and Notholt, J.: Impact of peatlands on carbon dioxide (CO_2) emissions from the Rajang River and

630   Estuary, Malaysia, Biogeosciences, 16, 17-32, https://doi.org/10.5194/bg-16-17-2019., 2019.

Ni, M., Li, S., Luo, J., and Lu, X.: CO_2 partial pressure and CO_2 degassing in the Daning River of the upper Yangtze River, China, Journal of Hydrology, 569, 483-494, https://doi.org/10.1016/j.jhydrol.2018.12.017, 2019.

Ran, L., Lu, X. X., Yang, H., Li, L., Yu, R., Sun, H., and Han, J.: CO_2 outgassing from the Yellow River

635   network and its implications for riverine carbon cycle, Journal of Geophysical Research: Biogeosciences, 120, 1334-1347, https://doi.org/10.1002/2015jg002982, 2015.

Ran, L., Li, L., Tian, M., Yang, X., Yu, R., Zhao, J., Wang, L., and Lu, X.: Riverine CO_2 emissions in the Wuding River catchment on the Loess Plateau: Environmental controls and dam impoundment impact, Journal of Geophysical Research: Biogeosciences, 122, 1439-1455,

640   https://doi.org/10.1002/2016JG003713, 2017a.

Ran, L., Lu, X. X., and Liu, S.: Dynamics of riverine CO_2 in the Yangtze River fluvial network and their implications for carbon evasion, Biogeosciences, 14, 2183-2198, https://doi.org/10.5194/bg-14-2183-2017, 2017b.

Ran, L., Lu, X., Fang, N., and Yang, X.: Effective soil erosion control represents a significant net carbon

645   sequestration, Scientific reports, 8, 12018, 2018.

Ran, Y., Li, X., Lu, L., and Li, Z.: Large-scale land cover mapping with the integration of multi-source information based on the Dempster–Shafer theory, International Journal of Geographical Information Science, 26, 169-191, 2012.

Rasera, M. d. F. F., Krusche, A. V., Richey, J. E., Ballester, M. V., and Victoria, R. L.: Spatial and temporal

650   variability of $p$$CO_2$ and CO_2 efflux in seven Amazonian Rivers, Biogeochemistry, 116, 241-259, https://doi.org/10.1007/s10533-013-9854-0, 2013.

Raymond, P. A., Zappa, C. J., Butman, D., Bott, T. L., Potter, J., Mulholland, P., Laursen, A. E., McDowell, W. H., and Newbold, D.: Scaling the gas transfer velocity and hydraulic geometry in streams and small rivers, Limnology and Oceanography: Fluids and Environments, 2, 41-53,

655   https://doi.org/10.1215/21573689-1597669, 2012.

Raymond, P. A., Hartmann, J., Lauerwald, R., Sobek, S., McDonald, C., Hoover, M., Butman, D., Striegl, R., Mayorga, E., and Humborg, C.: Global carbon dioxide emissions from inland waters, Nature, 503, 355-359, https://doi.org/10.1038/nature12760, 2013.

Reiman, J. H., and Xu, Y. J.: Diel Variability of pCO2 and CO2 Outgassing from the Lower Mississippi

660   River: Implications for Riverine CO2 Outgassing Estimation, Water, 11, 43, 2019a.

Reiman, J. H., and Xu, Y. J.: Dissolved carbon export and CO_2 outgassing from the lower Mississippi River – Implications of future river carbon fluxes, Journal of Hydrology, 578, 124093, https://doi.org/10.1016/j.jhydrol.2019.124093, 2019b.

Rocher‑Ros, G., Sponseller, R. A., Lidberg, W., Mörth, C. M., and Giesler, R.: Landscape process

665   domains drive patterns of CO2 evasion from river networks, Limnology and Oceanography Letters, 4, 87-95, 2019.

Sawakuchi, H. O., Neu, V., Ward, N. D., Barros, M. d. L. C., Valerio, A. M., Gagne-Maynard, W., Cunha, A. C., Less, D. F. S., Diniz, J. E. M., Brito, D. C., Krusche, A. V., and Richey, J. E.: Carbon dioxide emissions along the lower Amazon River, Frontiers in Marine Science, 4,

670 https://doi.org/10.3389/fmars.2017.00076, 2017.

Stets, E. G., Butman, D., McDonald, C. P., Stackpoole, S. M., DeGrandpre, M. D., and Striegl, R. G.: Carbonate buffering and metabolic controls on carbon dioxide in rivers, Global Biogeochemical Cycles, 31, 663-677, https://doi.org/10.1002/2016gb005578, 2017.

Tao, Z., Gao, Q., Wang, Z., Zhang, S., Xie, C., Lin, P., Ruan, X., Li, S., and Mao, H.: Estimation of
675 carbon sinks in chemical weathering in a humid subtropical mountainous basin, Chinese Science Bulletin, 56, 3774-3782, https://doi.org/10.1007/s11434-010-4318-6, 2011.

Teodoru, C., Nyoni, F., Borges, A., Darchambeau, F., Nyambe, I., and Bouillon, S.: Spatial variability and temporal dynamics of greenhouse gas (CO_2, CH_4, N_2O) concentrations and fluxes along the Zambezi River mainstem and major tributaries, Biogeosciences Discussion, 11, 16391-16445,
680 https://doi.org/10.5194/bgd-11-16391-2014, 2014.

Tian, M., Yang, X., Ran, L., Su, Y., Li, L., Yu, R., Hu, H., and Lu, X. X.: Impact of land cover types on riverine CO_2 outgassing in the Yellow River source region, Water, 11, 2243, https://doi.org/10.3390/w11112243, 2019.

Vonk, J. E., Mann, P. J., Davydov, S., Davydova, A., Spencer, R. G., Schade, J., Sobczak, W. V., Zimov,
685 N., Zimov, S., and Bulygina, E.: High biolability of ancient permafrost carbon upon thaw, Geophysical Research Letters, 40, 2689-2693, 2013.

Wanninkhof, R.: Relationship between wind speed and gas exchange over the ocean, Journal of Geophysical Research: Oceans, 97, 7373-7382, https://doi.org/10.1029/92JC00188, 1992.

Weiss, R. F.: Carbon dioxide in water and seawater: the solubility of a non-ideal gas, Marine Chemistry,
690 2, 203-215, https://doi.org/10.1016/0304-4203(74)90015-2, 1974.

Xuan, Y., Cao, Y., Tang, C., and Li, M.: Changes in dissolved inorganic carbon in river water due to urbanization revealed by hydrochemistry and carbon isotope in the Pearl River Delta, China, Environmental Science and Pollution Research, 10.1007/s11356-020-08454-4, 2020.

Yao, G., Gao, Q., Wang, Z., Huang, X., He, T., Zhang, Y., Jiao, S., and Ding, J.: Dynamics of CO_2 partial
695 pressure and CO_2 outgassing in the lower reaches of the Xijiang River, a subtropical monsoon river in China, Science of The Total Environment, 376, 255-266, https://doi.org/10.1016/j.scitotenv.2007.01.080, 2007.

Zhang, L., Qin, X., Liu, P., Huang, Q., Lan, F., and Ji, H.: Estimation of carbon sink fluxes in the Pearl River basin (China) based on a water–rock–gas–organism interaction model, Environmental Earth
700 Sciences, 74, 945-952, https://doi.org/10.1007/s12665-014-3788-2, 2015.

Zhang, S., Lu, X. X., Higgitt, D. L., Chen, C.-T. A., Han, J., and Sun, H.: Recent changes of water discharge and sediment load in the Zhujiang (Pearl River) Basin, China, Global and Planetary Change, 60, 365-380, https://doi.org/10.1016/j.gloplacha.2007.04.003, 2008.

Zhang, T., Li, J., Pu, J., and Yuan, D.: Carbon dioxide exchanges and their controlling factors in Guijiang
705 River, SW China, Journal of Hydrology, 578, 124073, https://doi.org/10.1016/j.jhydrol.2019.124073, 2019.

Zhang, W., Li, H., Xiao, Q., and Li, X.: Urban rivers are hotspots of riverine greenhouse gas (N2O, CH4, CO2) emissions in the mixed-landscape chaohu lake basin, Water Research, 189, 116624, https://doi.org/10.1016/j.watres.2020.116624, 2021.

710